JACS
JOURNAL OF THE AMERICAN CHEMICAL SOCIETY

ARTICLE

pubs.acs.org/JACS

Modulation of Electronic Couplings within Ru_2—Polyyne Frameworks

Bin Xi,[†] Isiah P.-C. Liu,[†] Guo-Lin Xu,[†] Mohommad M. R. Choudhuri,[‡] Maria C. DeRosa,[‡] Robert J. Crutchley,[‡] and Tong Ren*[,†]

[†]Department of Chemistry, Purdue University, West Lafayette, Indiana 47907, United States

[‡]Department of Chemistry, Carleton University, Ottawa, Ontario K1S 5B6, Canada

Supporting Information

ABSTRACT: Dimers of $[Ru_2(Xap)_4]$ bridged by 1,3,5-hexatriyn-diyl (Xap are 2-anilinopyridinate and its aniline substituted derivatives), $[Ru_2(Xap)_4]_2(\mu\text{-}C_6)$ (**1**), were prepared. Compounds **1** reacted with 1 equiv of tetracyanoethene (TCNE) to yield the cyclo-addition/insertion products $[Ru_2(Xap)_4]_2\{\mu\text{-}C{\equiv}CC(C(CN)_2){-}C(C(CN)_2)C{\equiv}C\}$ (**2**) and 1 equiv of $Co_2(dppm)(CO)_6$ to yield the η^2-Co_2 adducts to the middle C≡C bond, $[Ru_2(Xap)_4]_2(\mu\text{-}C_6)(Co_2(dppm)(CO)_4)$ (**3**). Voltammetric and spectroelectrochemical studies revealed that (i) two Ru_2 termini in **1** are sufficiently coupled with the mono-anion ($\mathbf{1}^-$) as a Robin—Day class II/III mixed valence species; (ii) the coupling between two Ru_2 is still significant but somewhat weakened in **3**; and (iii) the coupling between two Ru_2 is completely removed by the insertion of TCNE in **2**. The attenuation of electronic couplings in **2** and **3** was further explored with both the X-ray diffraction study of representative compounds and spin-unrestricted DFT calculations.

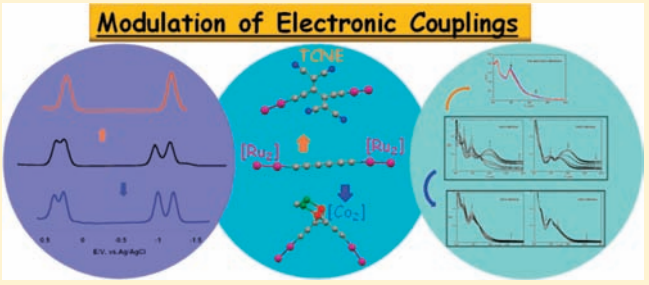

INTRODUCTION

Understanding and control of charge mobility within molecules and molecular assemblies is essential to chemical and materials sciences.[1] During the past decade, intense efforts have been focused on charge mobility on the nanoscale, especially molecules functioning as wires and active components of molecular devices.[2] Furthermore, the underpinning mechanism of charge transfer is intimately related to the study of photoinduced charge separation, which is key to the success of molecular photovoltaics.[3] Many molecular systems of a donor—bridge—acceptor arrangement have been investigated to understand the factors affecting intramolecular charge transfer, including thermodynamic driving force, attenuation by the bridge, and distance dependence.[4] In particular, bimetallic compounds of a σ-diyn—diyl bridge (Chart 1) have been studied extensively as the prototype of electronic and photonic wires,[5−7] where the rigidity of the C≡C—X—C≡C bridges enables precise control of [M]···[M] separation in addition to mediating charge (CT) and energy transfer (ET). Compounds of a polyyn—diyl bridge, namely —$(C{\equiv}C)_m$—, often exhibit exceptional CT and ET efficiencies, and recent examples include those with [M] as complexes of Fe,[8] Mn,[9] W,[10] Re,[11] Ru,[12] and Pt.[13]

Prior studies from our laboratories demonstrated facile electron/hole transfer across the polyyn—diyl chains in the $[Ru_2(ap)_4]_2(\mu\text{-}C_{2n})$ type compounds, where ap = 2-anilinopyridinate and n = 1−4 and 6.[14,15] Naturally, we are curious about the charge-transfer property of $[Ru_2(ap)_4]_2(\mu\text{-}C_{2n})$-type compounds with extended polyyn—diyl bridges ($n \geq 6$). Another interesting issue is whether it is possible to attenuate the charge-transfer processes

Chart 1. Bimetallic Diyn—Diyl Compounds

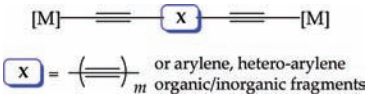

through modification of the polyyn—diyl bridges. Notable literature examples of attenuation include: (1) the control of electronic couplings between two $Ru(bipy)_3$ units through the open and closing of the dithienylethene bridge under photo stimuli;[16] (2) the pH-controlled mixed valency of [(edta)Ru(μ-benzotriazolate)-Ru(edta)]$^{3-}$;[17] and (3) the modulation of electronic couplings in $[Ru_2(\mu\text{-}C{\equiv}C{-}C{\equiv}C)]$ through the η^2 coordination of Cu(I) to the C≡C bond.[18] The scope of our study of $[Ru_2(ap)_4]_2(\mu\text{-}C_{2n})$-type compounds has often been limited by their solubility in common organic solvents. Two analogs of the ap ligand, 2-(3,5-dimethoxyanilino)pyridinate (DiMeOap) and 2-(3-^{t}butoxyanilino)pyridinate (^{t}BuOap), were introduced recently, and diruthenium compounds based on DiMeOap and ^{t}BuOap are much more soluble than those based on ap.[19,20] Furthermore, the improved solubility enables the preparation and separation of $[Ru_2(Xap)_4]_2(\mu\text{-}C_{2n})$ with n = 5−10, and the results will be described in a separate report.[21] $[Ru_2(ap)_4]_2(\mu\text{-}C_6)$ (**1a**) was reported in our prior study as a compound insoluble in common organic solvents and could not be characterized. Reported in this contribution are the preparation of **1a**'s soluble analogs

Received: May 31, 2011
Published: August 20, 2011

Chart 2. Compounds 1−3

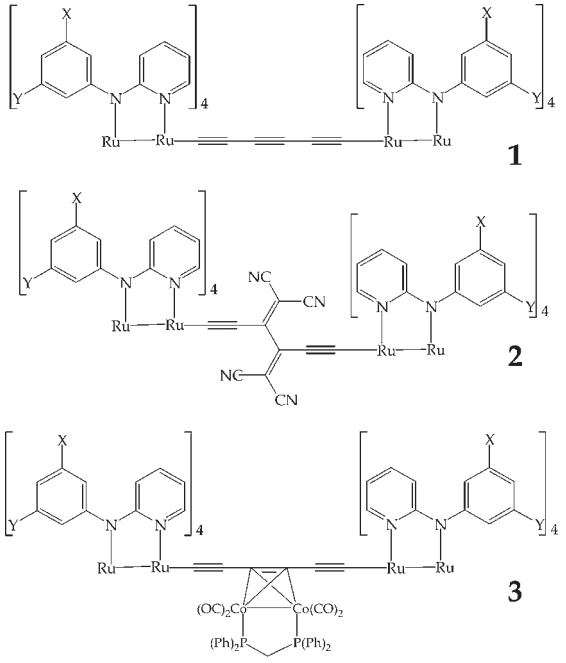

a: X = Y = H; **b**: X = Y = OMe; **c**: X = H, Y = ^{i}BuO

$[Ru_2(DiMeOap)_4]_2(\mu\text{-}C_6)$ (**1b**, Chart 2) and $[Ru_2(^{i}BuOap)_4]_2(\mu\text{-}C_6)$ (**1c**) and the products from the reactions between **1** and TCNE (compounds **2**) and between **1** and $Co_2(dppm)(CO)_6$ (compounds **3**) and the structural characterization of these compounds. Also described are the assessments of the electronic couplings in these compounds through voltammetric and spectroelectrochemical measurements and theoretical rationalization using DFT calculations.

RESULTS AND DISCUSSION

Syntheses. Similar to compound **1a**, compounds **1b** and **1c** were obtained from the reaction between $Ru_2(Xap)_4Cl$ and LiC_6Li in yields of 67 and 29%, respectively. Compound **1** reacted with TCNE in warm THF (~50 °C) to afford brownish products, which were identified as $[Ru_2(Xap)_4]_2\{\mu\text{-}C{\equiv}CC(C(CN)_2){-}C(C(CN)_2)C{\equiv}C\}$ (**2**) through both mass spectrometry and combustion analysis and a X-ray diffraction study of **2a**. As demonstrated in the prior studies of TCNE or 7,7,8,8-tetracyanoquinodimethane (TCNQ) addition to mononuclear polyynyls,[22−25] the formation of **2** was probably preceded with the formation of a [2 + 2] cyclo-addition intermediate. While the insertion of the metal bound C≡C unit into TCNE was feasible in mononuclear species,[22,24,25] the reactivity of **1** toward TCNE is restricted to the center C≡C bond due to the steric shielding of the Ru-bound C≡C units by the Xap ligands. Compound **1** reacted with $Co_2(dppm)(CO)_6$ in refluxing THF to yield $[Ru_2(Xap)_4]_2(\mu\text{-}C_6)[Co_2(dppm)(CO)_4]$ (**3**), typically a reddish-purple powder, as the major product. The successful preparation of the η^2-coordination adducts is similar to the early work of the addition of dicobalt clusters to organic and metallopolyynes.[25,26] All new compounds are quite stable under ambient conditions. Although the paramagnetism prevents characterization through NMR spectroscopy, compositions of **1**−**3** were ascertained through both the elemental analyses and the observation of corresponding molecular ions in fast atom bombardment mass spectrometry (FAB-MS) or electrospray ionization mass spectrometry (ESI-MS).

Structural Study. $[Ru_2(ap)_4]_2(\mu\text{-}C_{2n})$-type compounds are generally difficult to crystallize due to their low solubility and only those containing butadiyn−diyl (C_4) and octotetrayn−diyl (C_8) bridges have been structurally characterized.[15] With the more soluble DiMeOap ligand, X-ray quality crystals for compound **1b** were obtained from toluene and that of **3b** from THF. Compound **2a**, far more soluble than its parent compound **1a** due to the drastic change in structure, was also crystallized from THF. The structural plots of compounds **1b**, **2a**, and **3b** are shown in Figure 1, and the selected key metric parameters are collected in Table 1.

The overall structural features shown in Figure 1 are consistent with the expectation. Compound **1b** exhibits a linear $Ru_2{-}C_6{-}Ru_2$ backbone and contains a crystallographic inversion center that bisects the C_6 chain. In compound **2a**, both $Ru_2(ap)_4(C{\equiv}C)$ fragments are bent significantly downward from the C47−C47A bond to minimize steric crowding caused by the two dicyanomethine fragments, which are slightly buckled upward. There is a crystallographic two-fold axis passing through the middle of the C47−C47A bond and relating one-half of **2a** to the other half. The C47−C47A bond length is 1.50(1) Å, which is consistent with a C−C single bond indicated in Chart 2 and comparable to those found for the compounds derived from TCNE insertion into a hexatriyne fragment.[22] The η^2-coordination of the bulky $Co_2(CO)_4(dppm)$ fragment to the central C3−C4 bond in **3b** results in a very pronounced bending of the $Ru_2(ap)_4(C{\equiv}C)$ fragments. The C3−C4 bond length in **3b** (1.375(6) Å) is consistent with a C═C bond.

It is clear from Figure 1 that the coordination environments of the Ru_2 core in **1b**, **2a**, and **3b** are very similar to that observed in the prior studies of $Ru_2(ap)_4$-alkynyl compounds.[6] Most significantly, the Xap ligands adopt the (4, 0) arrangement with all aniline N coordinated to the Ru(II) center (4 site) and all pyridine N coordinated to the Ru(III) center (0 site), to the latter of which the alkynyl ligand is attached. The Ru−Ru distances in **1b** (2.3242(7) Å) and **3b** (2.3353(5) Å) are within the range found for other $Ru_2(Xap)_4$-alkynyl compounds (2.32−2.34 Å), while that in **2a** (2.3731(7) Å) is somewhat elongated. The elongation is likely the result of a stronger Ru−C bond in **2a**, which has the shortest Ru−C_α bond among the three structurally characterized compounds.

Electrochemical Studies. $Ru_2(ap)_4$(alkynyl)-type compounds usually display rich redox characteristics, and compounds **1**−**3** are no exception, as revealed in the differential pulse voltammograms (DPV) of compounds **1b**−**3b** shown in Figure 2. Cyclic voltammograms (CVs) were recorded for compounds **1**−**3**, but they are less informative because of the difficulty in resolving closely spaced waves. For this reason, all CVs and DPVs of compounds **2a**, **3a**, and **1c**−**3c** are provided in the Supporting Information. Similar to $[Ru_2(ap)_4]_2(\mu\text{-}C_{2n})$ compounds (n = 1, 2, and 4) reported earlier,[15] compound **1b** exhibits four one-electron processes in the window of −1.5 to + 1.0 V: a pair of oxidations (**A** and **B**, Scheme 1) and a pair of reductions (**C** and **D**) that are localized on the Ru_2 termini, and the appearance of these pairwise waves is indicative of a significant electronic coupling between two Ru_2 termini. In addition, compound **1b** also undergoes two one-electron reductions in the highly cathodic region (not shown), which are probably localized on the polyyn−diyl bridge.

dx.doi.org/10.1021/ja204813h |*J. Am. Chem. Soc.* 2011, 133, 15094–15104

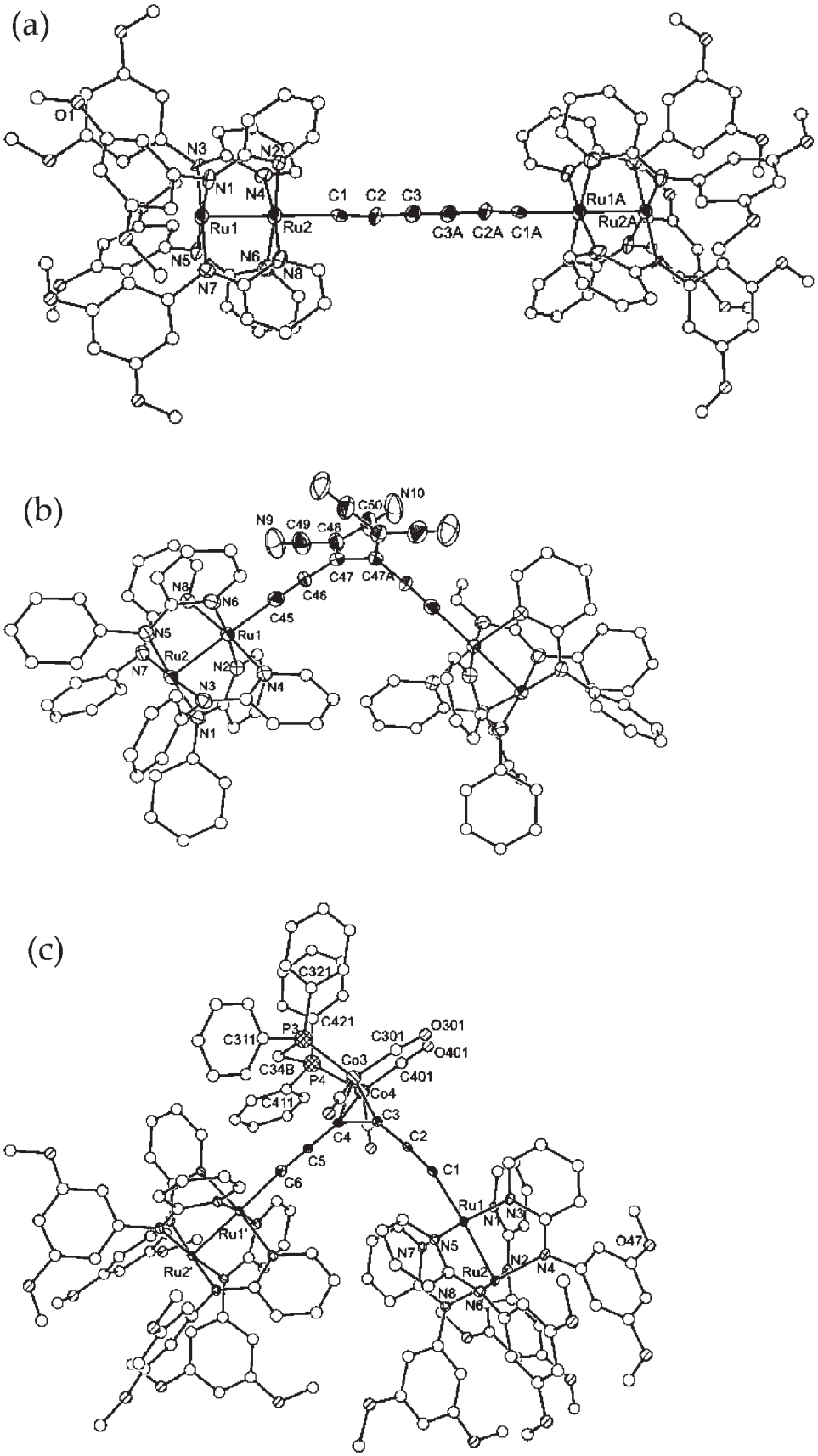

Figure 1. Structural plots of (a) $[Ru_2(DiMeOap)_4]_2(\mu\text{-}C_6)$ (**1b**), (b) $[Ru_2(ap)_4]_2(\mu\text{-}C_6)(TCNE)$ (**2a**), and (c) $[Ru_2(DiMeOap)_4]_2(\mu\text{-}C_6)[Co_2(dppm)(CO)_4]$ (**3b**).

dx.doi.org/10.1021/ja204813h |*J. Am. Chem. Soc.* 2011, 133, 15094–15104

Table 1. Selected Bond Lengths (Å) and Angles (°) for Compounds 1b, 2a, and 3b

1b		2a		3b			
Ru1−Ru2	2.3242(7)	Ru1−Ru2	2.3731(7)	Ru1−Ru2	2.3353(5)	Co3−Co4	2.4965(9)
Ru1−N1	2.048(5)	Ru1−N2	2.082(5)	Ru1−N1	2.098(4)	Co3−C3	1.947(4)
Ru1−N3	2.004(5)	Ru1−N4	2.080(5)	Ru1−N3	2.094(4)	Co3−C4	1.967(4)
Ru1−N5	2.054(5)	Ru1−N6	2.092(5)	Ru1−N5	2.124(4)	Co3−C301	1.786(5)
Ru1−N7	2.028(5)	Ru1−N8	2.069(5)	Ru1−N7	2.121(4)	Co3−P3	2.228(1)
Ru2−N2	2.097(5)	Ru2−N1	2.027(5)	Ru2−N2	2.054(4)	Co4−C401	1.773(5)
Ru2−N4	2.087(5)	Ru2−N3	2.029(5)	Ru2−N4	2.041(4)	Co4−C3	1.962(4)
Ru2−N6	2.090(5)	Ru2−N5	2.012(5)	Ru2−N6	2.039(4)	Co4−C4	1.964(4)
Ru2−N8	2.113(5)	Ru2−N7	2.003(5)	Ru2−N8	2.038(4)	Co4−P4	2.225(1)
Ru2−C1	2.110(6)	Ru1−C45	2.043(6)	Ru1−C1	2.065(5)	P3−C311	1.827(5)
C1−C2	1.199(8)	C45−C46	1.208(8)	C1−C2	1.226(6)	P3−C321	1.835(5)
C2−C3	1.355(9)	C46−C47	1.390(8)	C2−C3	1.403(6)	P3−C34B	1.849(4)
C3−C3A	1.19(1)	C47−C47A	1.45(1)	C3−C4	1.375(6)	P4−C421	1.833(5)
		C47−C48	1.373(9)	C4−C5	1.397(6)	P4−C34B	1.833(5)
		C48−C49	1.46(1)	C5−C6	1.234(6)	P4−C411	1.841(5)
		C48−C50	1.42(1)			C301−O301	1.145(5)
		C49−N9	1.12(1)			C401−O401	1.149(6)
		C50−N10	1.12(1)				
C1−Ru2−Ru1	177.9(2)	C45−Ru1−Ru2	178.7(2)	C1−Ru1−Ru2	175.8(1)	P4−C34B-P3	109.2(2)
C2−C1−Ru2	174.0(6)	C46−C45−Ru1	177.9(6)	C2−C1−Ru1	165.8(4)	C312−P3−C321	101.6(2)
C1−C2−C3	176.3(8)	C45−C46−C47	175.1(7)	C1−C2−C3	175.0(5)	C421−P4−C411	100.9(2)
C3A−C3-C2	176(1)	C46−C47−C47A	117.6(6)	C4−C3−C2	138.7(4)	C311−P3−Co3	119.8(2)
		C48−C47−C46	123.2(6)	C3−C4−C5	140.0(4)		
		C50−C48−C49	116.7(7)				

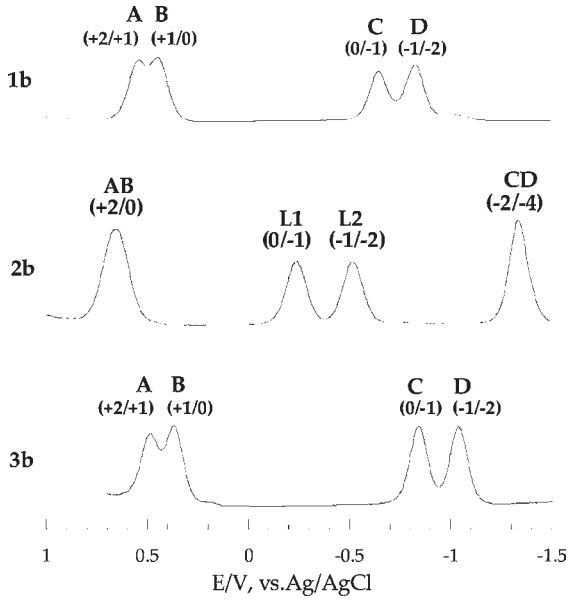

Figure 2. DPV of compounds **1b**−**3b** recorded in 0.20 M THF solution of Bu_4NPF_6.

It is clear from Figure 2 that compound **2b** is very different from compound **1b** in redox behavior. With the aid of spectroelectrochemistry (see the discussion below), the couple observed at 0.65 V is assigned as a two-electron oxidation of Ru_2 termini and labeled as **AB**. The significant anodic shift of the **AB** couple from the **A** and **B** couples in **1b** and **3b** is attributed to the enhanced

Scheme 1. Assignment of Reversible Redox Couples for 1b and 3b

$$[Ru_4]^{+2} \underset{A}{\overset{+e^-}{\rightleftharpoons}} [Ru_4]^{+1} \underset{B}{\overset{+e^-}{\rightleftharpoons}} [Ru_4]^{0} \underset{C}{\overset{+e^-}{\rightleftharpoons}} [Ru_4]^{-1} \underset{D}{\overset{+e^-}{\rightleftharpoons}} [Ru_4]^{-2}$$

electron deficiency via the insertion into TCNE. The one-electron ($1e^-$) couples at −0.25 (0/−1) and −0.52 V (−1/−2) are attributed to the stepwise reduction of the two dicyanomethine groups. The couple observed at −1.34 V (**CD**) is a two-electron ($2e^-$)reduction of the Ru_2 termini, and its cathodic shift from the **C** and **D** couples in **1b** is due to a much enhanced negative charge. The insertion of the $Ru_2-C_6-Ru_2$ moiety into TCNE clearly led to a complete switch off of the electronic coupling between two Ru_2 termini, as evidenced by the coalescence of stepwise $1e^-$ into $2e^-$ waves **AB** and **CD**. Similar disruption of the electronic coupling has been observed in related TCNE insertion products.[22] For instance, $FcC(C(CN)_2)-C(C(CN)_2)Fc$, derived from the reaction between TCNE and FcC≡CFc, displays a $2e^-$ Fc oxidation wave despite a very short Fc···Fc separation (3.15 Å).[27]

The DPV of compound **3b** is quite similar to that of **1b** in having pairwise oxidations and reductions in the same potential window. Similar to the case of **1b**, these couples are also Ru_2-based since the $Co_2(dppm)(CO)_4$ fragment is redox inactive in this potential window. Compared to **1b**, all couples of **3b** are cathodically shifted, reflecting the donor nature of the $Co_2(dppm)(CO)_4$ fragment. Interestingly, the potential differences for the pairwise couples (ΔE_p, see Table 2) in **3b** are larger than those for the corresponding couples in **1b**. While the ΔE_p might

dx.doi.org/10.1021/ja204813h |J. Am. Chem. Soc. 2011, 133, 15094–15104

Table 2. Electrochemical Data (V) for Compounds 1−3 from DPV Studies

compound	+2/+1	+1/0	ΔE_p	0/−1	−1/−2	$\Delta E_p'$	−2/−3	−3/−4
1b	0.54	0.44	0.10	−0.65	−0.83	0.18	−1.81	−2.08
1c	0.54	0.44	0.10	−0.67	−0.87	0.20	−1.85	−2.14
2a	0.66 ($2e^-$)		NA	−0.25	−0.53		−1.32 ($2e^-$)	
2b	0.65 ($2e^-$)		NA	−0.25	−0.52		−1.34 ($2e^-$)	
2c	0.66 ($2e^-$)		NA	−0.27	−0.55		−1.34 ($2e^-$)	
3a	0.50	0.37	0.13	−086	−1.05	0.19	NA	
3b	0.49	0.37	0.12	−0.84	−1.04	0.20	NA	
3c	0.49	0.35	0.14	−0.87	−1.07	0.20	NA	

be indicative of stronger coupling in **3b**, the analysis of intervalence bands (see below) shows that coupling is greater for type **1** compounds. The apparent contradiction is rooted in that ΔE_p is proportional to the free energy of comproportionation ΔG_c, whose magnitude is usually determined by four factors:

$$\Delta G_c = \Delta G_s + \Delta G_r + \Delta G_e + \Delta G_i$$

where ΔG_s reflects the statistical distribution of the comproportionation equilibrium, ΔG_e accounts for the electrostatic repulsion of the two like-charged metal centers, ΔG_i is an inductive factor dealing with competitive coordination of the bridging ligand by the metal ions, and ΔG_r is the free energy of resonance exchange (or metal−metal coupling).[28] For compounds discussed herein, ΔG_e is expected to vary significantly for **2** and **3** because of the term's dependence on the distance between charged centers. The closest distance between ruthenium centers in **1** is 10.5 Å, while for **2** and **3** it is 8.4 and 7.9 Å, respectively. Because of the double bond in the bridge, **3** has a rigid structure in solution, and this may favor contributions from other factors, such as solvation and ion pairing.[29]

Potential data obtained for all of compounds **1**−**3**, except insoluble **1a**, are listed in Table 2, while the CVs for all compounds and DPVs for **1c**, **2a**, **2c**, **3a**, and **3c** are provided in the Supporting Information. It is clear from Table 2 that the potentials for the same couple are nearly identical among the same type of compounds. This is consistent with our prior studies, which indicate that the modification of the ap ligand with a RO-substituent at the aniline ring causes very minimal changes in both structural and electronic properties.[19,30]

Vis-NIR Absorption Spectra. Compounds **1**−**3** are strong absorbers in the vis-NIR region and typical spectra recorded in THF for **1c**, **2a** and **3c** are shown in Figure 3. Compound **1c** features an intense peak at 766 nm with a shoulder at ca. 950 nm and another pair of peaks at 597 (intense) and 470 nm. The lower energy pair is of a $\delta \rightarrow \delta^*$ transition origin and gained intensity from their partial metal-to-ligand charge transfer (MLCT) character due to the mixing between the δ^* and π(N) orbitals.[15,31] The higher energy pair is the dipole-allowed $\pi(N) \rightarrow \pi^*/\delta^*(Ru_2)$ transition. The pairwise appearance is an indicator of significant orbital mixings between two Ru_2 termini due to the delocalization across the C_{2n} bridge, as discussed previously.[15] The spectrum of **3c** is very similar to that of **1c** in both peak positions and intensity. However, the pairwise feature in **3c**, although discernible, is not as well-defined as in **1c**. We surmise that this "smearing" is due to the low symmetry of the $Ru_2-C_{2n}-Ru_2$ backbone in **3c** instead of a reduced electronic coupling. The spectrum of **2a** is very different from the other two in both lower intensity and lack of the pairwise feature, which is attributed to the absence of the Ru_2-Ru_2 coupling (see discussion below).

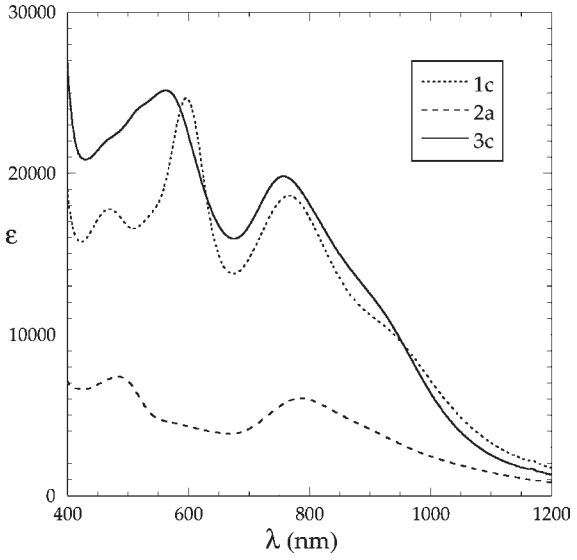

Figure 3. Vis-NIR spectra of compounds **1c**, **2a**, and **3c** recorded in THF.

*Spectroelectrochemical Study of **1c** and **3c**.* Representative spectroelectrochemistry on type **1**, **2**, and **3** compounds was performed on THF solutions of compounds **1c**, **2a**, and **3c**, and the spectral changes (vide infra) showed good reversibility with at least 95% return to starting compound absorbance.

In Figure S4a, Supporting Information, the oxidation to $\mathbf{1c}^+$ results in a decrease in the absorbance of the band at 597 nm and an increase in NIR absorbance with a band maximum at 992 nm and a very broad shoulder at 1575 nm. Further oxidation to $\mathbf{1c}^{2+}$ (Figure S4b, Supporting Information) shows an increase in absorbance of a band at 800 nm and only a slight drop in NIR absorbance between 1500 and 1750 nm. The latter may be due to a very weak intervalence transition associated with $\mathbf{1c}^+$.

In Figure 4a, reduction to $\mathbf{1c}^-$ results in a dramatic decrease in the absorbance of the bands at 597 and 800 nm and the growth of a band centered at 1200 nm and a broad absorption at approximately 1900 nm. As shown in Figure 4b, these two bands are lost upon reduction to $\mathbf{1c}^{2-}$ and are therefore assigned to intervalence transitions of $\mathbf{1c}^-$. Deconvolution of these bands, assuming two Gaussian band shapes gave for the high-energy intervalence band, ν_{max} = 8180 cm^{-1}, $\nu_{1/2}$ = 2790 cm^{-1}, and ε_{max} = 18 100 $M^{-1}cm^{-1}$ and for the low-energy intervalence band, ν_{max} = 5180 cm^{-1}, $\nu_{1/2}$ = 2020 cm^{-1}, and ε_{max} = 7360 $M^{-1}cm^{-1}$. The half widths predicted by the Hush model ($\nu_{1/2}(Hush) = (2310\nu_{max})^{1/2}$)[32] are 4350 and 3460 cm^{-1} for the higher and lower energy bands, respectively. On the basis of the $\nu_{1/2}$ data, the corresponding $\Gamma(1 - \nu_{1/2}/\nu_{1/2}(Hush))$ values are 0.36 and 0.42, indicating that $\mathbf{1c}^-$ is a species at the Robin-Day class II−III transition according to Brunschwig, Creutz, and Sutin.[33] These intervalence bands are weaker in intensity and broader than those observed for the analogous mixed-valence complex incorporating the butadiyn−diyl bridge,[15] which is a consequence of the weaker coupling between the $Ru_2(ap)_4$ moieties because of the greater separation imposed by the hexadiyn−diyl bridge in **1c**.

Spectroelectrochemical oxidations of **3c** to $\mathbf{3c}^+$ and $\mathbf{3c}^{2+}$ (Figure S5a and b, Supporting Information, respectively) show much the same behavior as those of **1c**; the initial oxidation

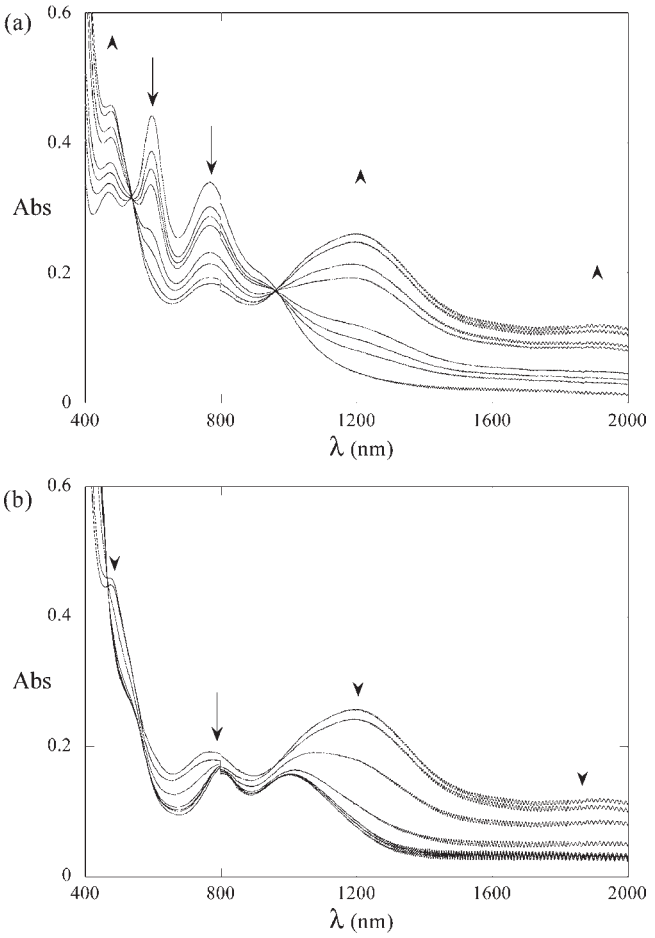

Figure 4. Spectroelectrochemical reduction of complex **1c** in THF and 0.2 M TBAH: (a) 0/−1 and (b) −1/−2 reductions, respectively.

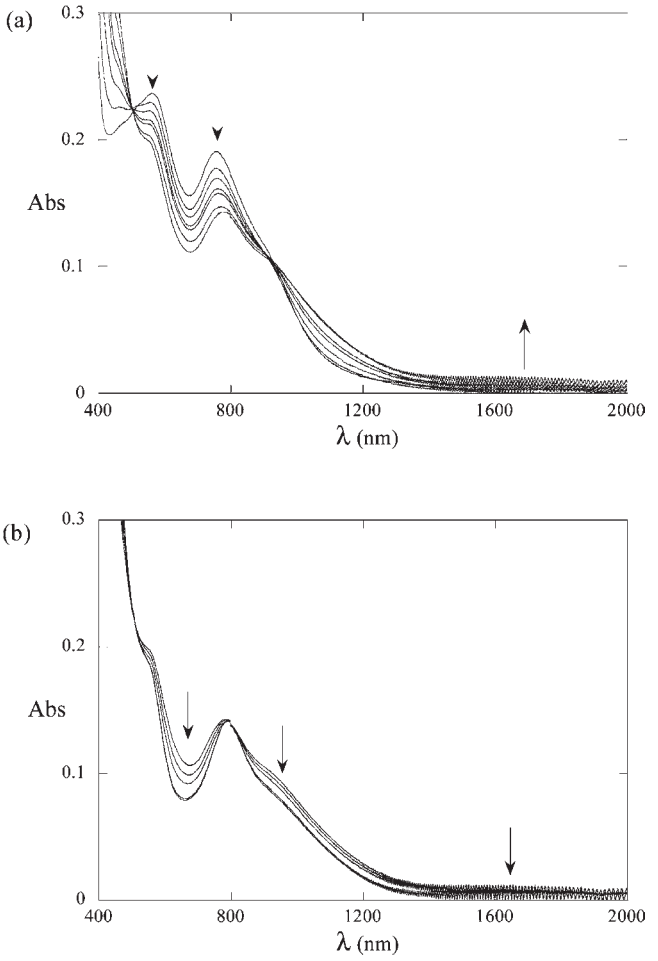

Figure 5. Spectroelectrochemical reduction of compound **3c** in THF and 0.2 M TBAH, (a) 0/−1 and (b) −1/−2 reductions, respectively.

results in the growth of a significant NIR absorbance, while the second oxidation shows only a slight decrease in the NIR absorbance at approximately 1800 nm, which may be due to a very weak intervalence transition. A significant difference between these two complexes can be seen by comparing the reduction spectroelectrochemistry (Figures 4 and 5).

In Figure 5a, the reduction to the mixed-valence compound $\mathbf{3c}^-$ shows a decrease and broadening of the absorbance of the band centered at 800 nm and a very weak NIR absorption centered at 1700 nm. Further reduction to $\mathbf{3c}^{2-}$ (Figure 5b) shows a decrease in this absorption band and a narrowing of the band centered at 800 nm. The absorbance centered at 1700 nm in the spectrum of $\mathbf{3c}^-$ is suggested to be a weak intervalence transition. It is sufficiently separated from the relatively strong band centered at 800 nm to be deconvoluted with confidence. Assuming a single Gaussian band, deconvolution gave intervalence band data: $\nu_{max} = 5880\ cm^{-1}$, $\nu_{1/2} = 4080\ cm^{-1}$, and $\varepsilon_{max} = 950\ M^{-1}\ cm^{-1}$. The difference in intervalence band properties between $\mathbf{1c}^-$ and $\mathbf{3c}^-$ is noteworthy. For $\mathbf{3c}^-$, the IT band is slightly broader than predicted by the Hush model ($\nu_{1/2}$(Hush) = $3690\ cm^{-1}$) and is therefore consistent with a weakly coupled mixed-valence system (Robin Day class I−II). As mentioned above, the IT bands of $\mathbf{1c}^-$ are far narrower, which qualify $\mathbf{1c}^-$ as a Robin-Day class II−III mixed valent ion.[33] It seems reasonable to suggest that the difference in coupling between **1c** and **3c** is a consequence of the nature of the bridge between the $Ru_2(ap)_4$

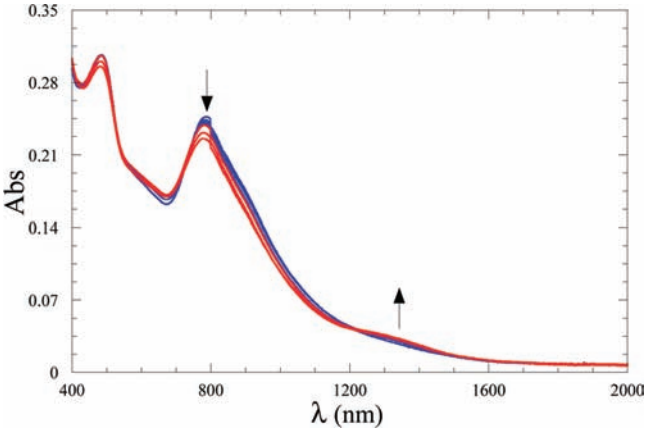

Figure 6. Spectral changes of **2a** upon the first (blue, 0/−1) and second (red, −1/−2) reductions; all recorded in THF and 0.2 M TBAH.

termini: it consists of three conjugated —C≡C— moieties in **1c**, and —C≡C—C═C—C≡C— in **3c**. The relatively poor mixing between ethylene and acetylene moieties is suggested to cause the weaker coupling of $\mathbf{3c}^-$. When the ethylene moiety is replaced by a saturated link, mixed-valence coupling should be even more attenuated, and this was shown by the overlap of oxidation

dx.doi.org/10.1021/ja204813h |J. Am. Chem. Soc. 2011, 133, 15094–15104

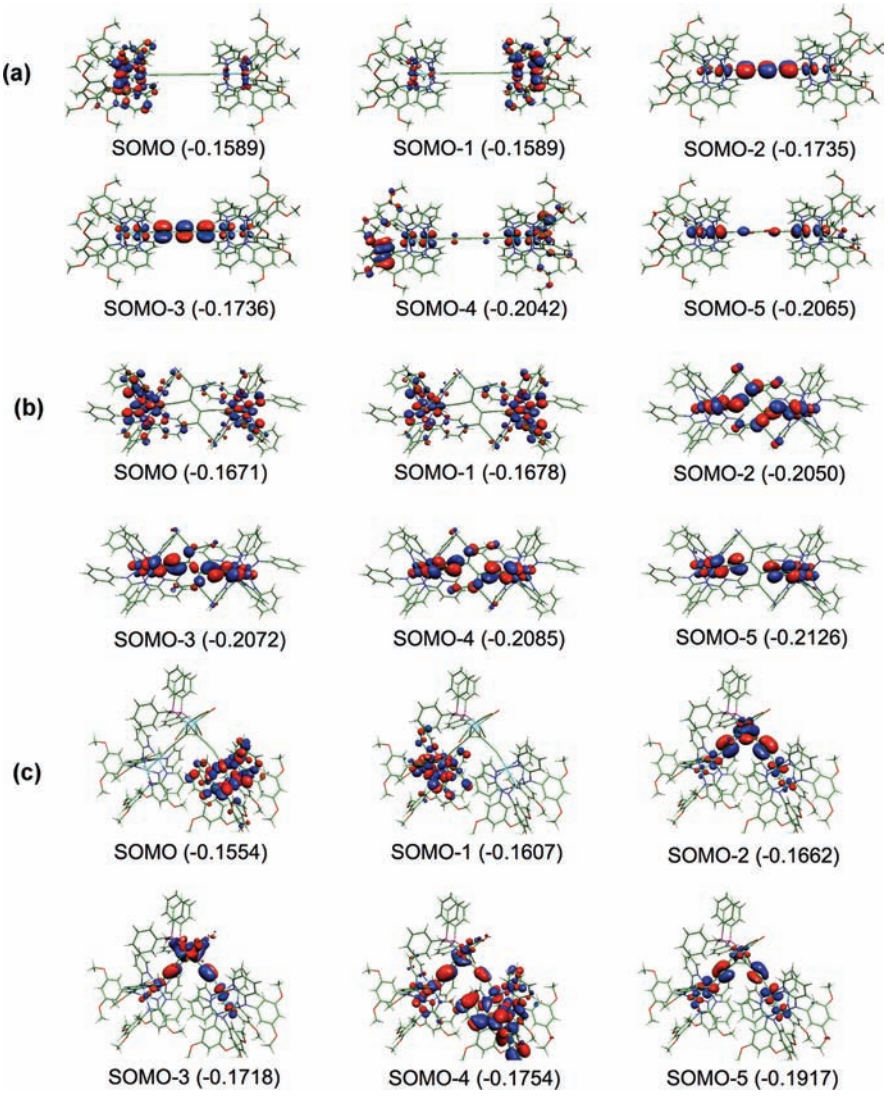

Figure 7. Singly occupied molecular orbitals and energies (in hartree) of compounds (a) **1b**, (b) **2a**, and (c) **3b**.

couples seen for **2b** in Figure 2. The reduction spectroelectrochemistry of **2a** is shown in Figure 6, while the oxidation spectroelectrochemistry is provided in Figure S6, Supporting Information.

In Figure S6, Supporting Information, two-electron oxidation of **2a** results in significant changes in the visible region, but there was no appearance of a NIR band that could be assigned to an intervalence transition. Moreover, the pattern of spectral changes closely tracks that of the oxidation of $Ru_2(ap)_4(C_2SiMe_3)$,[15] which reaffirms the assignment of **AB** as the simultaneous oxidation of both $Ru_2(ap)_4$ units that are electronically "insulated" from each other. Upon the first (0/−1) and second (−1/−2) reductions (Figure 6), there was neither a quenching of the 800 nm band, as observed during the reduction of $Ru_2(ap)_4(C_2SiMe_3)$,[15] nor the appearance of an intense intervalence charge-transfer band, as observed for the reduction of **1c** (Figure 4). Hence, both the 0/−1 and −1/−2 couples are localized on the ligand bridge and most likely on the dicyanomethylene groups. The voltammetric behavior of **2a** is in stark contrast to the voltammetric behavior of both compounds **1** and other previously studied $[Ru_2(ap)_4]_2(\mu\text{-}C_{2n})$ (n = 1, 2, 4, and 6) compounds,[15] which all exhibit stepwise Ru_2-centered reductions. Thus, the insertion of **1** into TCNE has resulted in a junction that "insulates" the two $Ru_2(ap)_4$ units from both the hole (oxidation) and electron (reduction) transfer.

DFT Study. In order to gain further understanding of the nature of electronic couplings in compounds **1**−**3**, single-point spin-unrestricted DFT calculations were performed on the compounds **1b**, **2a**, and **3b** based on their respective X-ray structures without truncation. Monoalkynyl-$Ru_2(Xap)_4$ compounds generally have three unpaired electrons originated from the $\sigma^2\pi^4\delta^2\pi^{*2}\delta^{*1}$ configuration.[6,20,34] Since the δ^* orbital is based on the Ru d_{xy} orbital, it will not interact with the π-orbitals of the axial alkynyl ligand due to orbital orthogonality, and the unpaired δ^* electron can be considered as a localized electron. The π^* orbitals are composed of Ru d_{xz} and d_{yz} orbitals, which can overlap effectively with the π(C≡C) of the axial alkynyl ligand. The π^* electrons can be delocalized onto the polyyndiyl bridge and be responsible for the electronic coupling between two Ru_2 termini. Thus, the degree of electronic coupling between two Ru_2 termini may be estimated intuitively by considering the composition of magnetic orbitals contributed by Ru π^* orbitals and the bridging ligand (superexchange).[35]

Six magnetic orbitals for each of compounds **1b**, **2a**, and **3b** are depicted in Figure 7. In all cases, the SOMO and SOMO-1 are composed of the δ^* orbitals of the Ru_2(II,III) moieties without the contribution of the polyyn−diyl ligand. These electrons are localized on two ends of the molecule and do not contribute to the electronic coupling. Because of the weak interaction between these two Ru_2(II,III) fragments, the singly occupied molecular orbital (SOMO) and SOMO-1 are almost degenerate. The SOMO and SOMO-1 in both **1b** and **3b** also appear dissymmetric, which is likely caused by the lower symmetry of X-ray structures. The calculated lowest unoccupied molecular orbitals (LUMOs) up to LUMO+3 are provided in the Supporting Information (Figure S7). It is noteworthy that while the calculated LUMO and LUMO+1 are Ru_2-localized for **1b** and **3b**, those of **2a** are primarily delocalized over two dicyanomethine fragments, confirming the assignment of the first and second reductions observed in compounds **2**.

The SOMO-2−SOMO-5 of compounds **1b**, **2a**, and **3b** are based on the combination of the $\pi^*(Ru_2)$ orbitals with the π orbitals of the polyyn−diyl bridge, which are of antibonding nature (Figure 7). This is consistent with the fact that the π-interaction in metal−alkynyl bonding is dominated by the filled−filled type, pointed out first by Lichtenberger.[36] For compound **1b**, both the SOMO-2 and SOMO-3 display extensive mixings between $\pi^*(Ru_2)$ and all three π(C≡C) across the C_6 bridge, while the SOMO-4 and SOMO-5 contain much less contribution from the C_6 bridge. For compound **3b**, although intimate mixings between $\pi^*(Ru_2)$ and the π(C≡C) of Ru-bound acetylene unit are significant in the SOMO-2−SOMO-5, the contribution from the π orbitals of the middle C_2 unit is less clear because of the η^2 coordination of Co_2.

For compound **2a**, the situation is different. The X-ray structural study revealed that: (i) the middle C−C (C3−C3A) bond is a single bond after the insertion into TCNE; and (ii) the bridging ligand is twisted around the middle C−C bond. The latter feature forces the π orbitals on the C1−C2 and C1A−C2A bonds to become quasi-orthogonal. The π-delocalization pathway found **1b** and **3b** no longer exists, and the odd electron (hole) can only be localized on one-half of the molecule (Figure 7b), which effectively eliminates the possibility of electronic coupling between two Ru_2 termini.

CONCLUSIONS

It is demonstrated through voltammetric and spectroelectrochemical studies that the electronic coupling across the [M]—$(C{\equiv}C)_{2n}$-—[M] framework can be either attenuated by the coordination of a Co_2 cluster or completely interrupted by the insertion into TCNE. Both the X-ray study and DFT calculations offer additional insights and detailed orbital pictures of superexchange pathways. In contrast to the type **1** compounds, the spectroelectrochemical study of type **3** compounds did not reveal a significant IVCT band despite having a slightly larger comproportionation constant. It was suggested that for type **3** compounds other factors aside from resonance exchange contribute to the magnitude of the comproportionation constant. The attenuation of electronic couplings uncovered herein is analogous to that caused by cross-conjugation, which has been proposed as a mechanism for increasing the dynamic range of conductance switching.[37] Our laboratories are further exploring the molecular wire characteristics of type **2** and **3** compounds through nanojunction measurements.

EXPERIMENTAL SECTION

Tetracyanoethene was purchased from ACROS, *n*-BuLi in hexanes from Aldrich, and silica gel from Merck. $[Ru_2(ap)_4]_2(\mu\text{-}C_6)$ (**1a**),[15] $Ru_2(DiMeOap)_4Cl$,[19] $Ru_2(^tBuOap)_4Cl$,[20] $Co_2(dppm)(CO)_6$,[38] and 1,6-bis(trimethylsilyl)-1,3,5-hexatriyne[39] were prepared according to the literature procedures. Unless specified, all syntheses were performed using standard Schlenk techniques under a nitrogen atmosphere. THF was distilled over Na/benzophenone under an N_2 atmosphere prior to use. Vis-NIR spectra were obtained in THF with a JASCO V-670 UV−vis NIR spectrophotometer. Infrared spectra were recorded on a JASCO FT/IR-ATR 6300 spectrometer. Elemental analysis was performed by Atlantic Microlab, Norcross, GA. Both cyclic and differential pulse voltammograms were recorded in 0.2 M $(n\text{-}Bu)_4NPF_6$ solution (THF, N_2-degassed) on a CHI620A voltammetric analyzer with a glassy carbon working electrode (diameter = 2 mm), a Pt-wire auxiliary electrode and a Ag/AgCl reference electrode. The concentration of diruthenium species is always 1.0 mM. The ferrocenium/ferrocene couple was observed at 0.591 V (vs. Ag/AgCl) under the experimental conditions.

Synthesis of $[Ru_2(DiMeOap)_4]_2(\mu\text{-}C_6)$ (1b). To 20 mL THF solution of $TMSC_6TMS$ (0.055 g, 0.25 mmol) was added 0.35 mL of 1.6 M BuLi at −78 °C, and the reaction mixture was slowly warmed to room temperature and stirred for 2 h. The resultant dark-brown solution was transferred to a 60 mL THF solution of $Ru_2(DiMeOap)_4Cl$ (0.634 g, 0.55 mmol). The reaction mixture was stirred at room temperature for 2 h and filtered through a 2-cm silica gel pad (deactivated with Et_3N). The filtrate was dried, and the residue was washed with Et_2O, CH_3OH, and hexanes to yield a dark-blue solid. Further recrystallization from THF/hexanes yielded the analytically pure compound **1b** (0.42 g, 67% based on Ru). Data for **1b**: R_f = 0.37 (THF/hexanes/Et_3N = 1/2/0.1, v/v/v). Anal. for $C_{110}H_{104}N_{16}O_{16}Ru_4$ found (calcd): C, 57.28 (57.19); H, 4.65 (4.51); N, 9.28 (9.71); ESI-MS (*m/e*, based on ^{101}Ru): 2309 ($[M+H]^+$); Vis-NIR, λ_{max}(nm, $\varepsilon(M^{-1}cm^{-1})$): 950(sh), 768(14 100), 598(17 600), 472(13 600); IR, υ/cm^{-1}: 2138 (w, C≡C), 1963 (w, C≡C); μ_{eff} (294 K): 4.55 μ_B (μ_{eff}/Ru_2: 3.22 μ_B). Electrochemical, $E_{1/2}$/V, E_p/V, $i_{backward}/i_{forward}$: A, 0.58 (E_{pa}); B, 0.43 (E_{pc}); C, −0.68, 0.062, 0.75; D, −0.86, 0.063, 1.18; E, −1.83, 0.060, 1.02; F, −2.10, 0.059, 0.79.

Synthesis of $[Ru_2(^tBuOap)_4]_2(\mu\text{-}C_6)$ (1c). Compound **1c** was prepared using the same procedure as that for **1b** with $Ru_2(DiMeOap)_4Cl$ being replaced by $Ru_2(^tBuOap)_4Cl$ in 29% yield. Data for **1c**: R_f = 0.55 (THF/hexanes/Et_3N = 1/3/0.1, v/v/v). Anal. for $C_{126}H_{136}N_{16}O_8Ru_4$ found (calcd): C, 62.63 (62.82); H, 5.85 (5.65); N, 9.05 (9.31). Vis-NIR, λ_{max}(nm, $\varepsilon(M^{-1}cm^{-1})$): 950(sh), 766(18 600), 597(24 700), 470(17 800). IR, υ/cm^{-1}: 2124 (w), 2063 (w), 1997 (w). Electrochemical, $E_{1/2}$/V, E_p/V, $i_{backward}/i_{forward}$: A, 0.57 (E_{pa}); B, 0.40 (E_{pc}); C, −0.70, 0.082, 0.85; D, −0.86, 0.070, 1.20.

Synthesis of $[Ru_2(ap)_4]_2\{\mu\text{-}C{\equiv}CC(C(CN)_2)—C(C(CN)_2)C{\equiv}C\}$ (2a). Compound **1a** (0.180 g, 0.10 mmol) was suspended in 40 mL THF, to which was added TCNE (0.013 g, 0.10 mmol) at room temperature. A clear solution was obtained immediately upon the addition of TCNE and stirred under N_2 for 30 min. After solvent removal, the residue was washed with methanol. Further recrystallization from CH_2Cl_2/hexanes yielded a brown crystalline solid (0.170 g, 87% based on Ru). Data for **2a**: Anal. for $C_{100}H_{72}N_{20}Ru_4\cdot 2CH_2Cl_2$ found (calcd): C, 58.24(57.57); H, 3.65(3.57); N, 13.17(13.31); FAB-MS (*m/e*, based on ^{101}Ru): 1958 ($[M]^+$); Vis-NIR, λ_{max}(nm, $\varepsilon(M^{-1}cm^{-1})$): 787(7400), 485(6100); IR, υ/cm^{-1}: 2217 (w, C≡C), 1972(s, C≡N); Electrochemical, $E_{1/2}$/V, E_p/V, $i_{backward}/i_{forward}$: A and B, 0.63, 0.091, 1.00; L1, −0.26, 0.058, 0.79; L2, −0.55, 0.057, 1.00; C and D, −1.33, 0.059, 1.00. χ_{mol}(corrected) = 9.57 × 10^{-3} emu, μ_{eff} = 4.78 μ_B.

Synthesis of $[Ru_2(DiMeOap)_4]_2\{\mu\text{-}C{\equiv}CC(C(CN)_2)—C(C(CN)_2)C{\equiv}C\}$ (2b). To a 40 mL THF solution of **1b** (0.300 g, 0.13 mmol) was added TCNE (0.033 g, 0.26 mmol) at room temperature.

Table 3. Crystallographic Parameters for Compounds $1b \cdot 2C_7H_8$, $2a \cdot 4THF \cdot 2H_2O$, and $3b \cdot 3THF$

	$1b \cdot 2C_7H_8$	$2a \cdot 4THF \cdot 2H_2O$	$3b \cdot 3THF$
empirical formula	$C_{138}H_{120}N_{16}O_{16}Ru_4$	$C_{116}H_{108}N_{20}O_6Ru_4$	$C_{151}H_{150}Co_2N_{16}O_{23}P_2Ru_4$
formula weight	2662.78	2282.50	3141.07
space group	$P\bar{1}$	C2/c	$P\bar{1}$
a (Å)	13.6619(9)	16.2323(16)	18.7179(8)
b (Å)	13.8526(10)	35.319(4)	22.1686(14)
c (Å)	18.2493(12)	19.3815(19)	22.2364(14)
α (°)	67.7420(10)		114.086(3)
β (°)	82.7380(10)	95.983(2)	98.165(2)
γ (°)	81.480(2)		101.781(2)
V (Å^3)	3151.8(4)	11 051(19)	7979.7(8)
Z	1	8	2
d_{calc} (g cm^{-3})	1.403	1.331	1.307
μ (mm^{-1})	0.541	0.596	0.648
T (K)	300(2)	300(2)	150
$R1$, $wR2$	0.059, 0.149	0.052, 0.139	0.069, 0.124

The color of the reaction mixture changed from dark-blue to dark-brown immediately upon the addition of TCNE. The reaction mixture was warmed to ca. 50 °C for 1 h. After solvent removal, the residue was washed with methanol and hexanes to yield a dark-brown solid, which was recrystallized from THF/hexanes to yield a brown solid (0.27 g, 86% based on Ru). Data for **2b**: R_f = 0.13 (THF/hexanes/Et_3N = 1/2/0.1, v/v/v). Vis-NIR, λ_{max} (nm, ε(M^{-1} cm^{-1})): 791(6,100), 485 (7,600). Anal. for $C_{116}H_{104}N_{20}O_{16}Ru_4 \cdot 6CH_2Cl_2 \cdot 3H_2O$ found (calcd): C, 48.48 (48.87); H, 3.87 (4.07); N, 9.79 (9.35); ESI-MS (m/e, based on ^{101}Ru): 2439 ([M + H]$^+$); IR, υ/cm^{-1}: 2215 (w, C≡C), 1967(s, C≡N); μ_{eff} (294 K): 5.50 μ_B (μ_{eff}/Ru_2: 3.89 μ_B). Electrochemical, $E_{1/2}$/V, E_p/V, $i_{backward}$/$i_{forward}$: A and B, 0.62, 0.113, 0.99; L1, −0.26, 0.109, 0.83; L2, −0.54, 0.086, 0.76; C and D, −1.37, 0.111, 1.70.

Synthesis of $[Ru_2(^iBuOap)_4]_2\{\mu$-C≡CC(C(CN)$_2$)—C(C(CN)$_2$)-C≡C$\}$ (2c). Compound **2c** was prepared using the same procedure as that for **2a** with $[Ru_2(ap)_4]_2(\mu$-$C_6)$ being replaced by $[Ru_2(^iBuOap)_4]_2(\mu$-$C_6)$ in 66% yield. Data for **2c**: R_f = 0.50 (THF/hexanes/Et_3N = 1/3/0.1, v/v/v). Vis-NIR, λ_{max} (nm, ε(M^{-1} cm^{-1})): 790 (17 000), 580 (sh), 490 (28 0600). Anal. for $C_{132}H_{136}N_{20}O_8Ru_4$, found (calcd): C, 62.76-(62.49); H, 5.41(5.37); N, 10.94(11.05). IR, υ/cm^{-1}: 2218 (w), 2097 (w), 1975(s); Electrochemical, $E_{1/2}$/V, E_p/V, $i_{backward}$/$i_{forward}$: A and B, 0.63, 0.086, 1.03; L1, −0.30, 0.065, 0.86; L2, −0.57, 0.065, 1.24; C and D, −1.36, 0.060, 0.50.

Synthesis of $[Ru_2(ap)_4]_2(\mu$-$C_6)[Co_2(CO)_4(dppm)]$ (3a). Compound **1a** (0.160 g, 0.087 mmol) was suspended in 40 mL THF, to which was added $Co_2(CO)_6$(dppm) (0.160 g, 0.18 mmol). After refluxing for 2 h, the reaction mixture changed from dark-blue to dark-violet. After solvent removal, the residue was washed with methanol and hexanes. Further purification on a silica gel column deactivated by 10% Et_3N in hexanes using a linear gradient of eluents (hexanes/ethyl acetate, 10/1−5/1, v/v) afforded **3a** as a dark-violet solid (0.040 g, 19%). Data for **3a**: R_f = 0.37 (THF/hexanes/Et_3N = 1/2/0.1, v/v/v). Anal. for $C_{123}H_{94}N_{16}O_4P_2Ru_4$-$Co_2$, found (calcd): C, 60.18(60.39); H, 3.74(3.85); N, 9.01(9.16). Vis-NIR, λ_{max} (nm, ε(M^{-1} cm^{-1})): 950(sh), 753(13 400), 561(15 700), 465(sh). IR, υ/cm^{-1}: 2016 (w), 1995 (w), 1968 (w). Electrochemical, $E_{1/2}$/V, E_p/V, $i_{backward}$/$i_{forward}$: E_{pa}(A), 0.51; E_{pa}(B), 0.32; C, −0.89, 0.078, 0.80; D, −1.07, 0.053, 1.24.

Synthesis of $[Ru_2(DiMeOap)_4]_2(\mu$-$C_6)[Co_2(CO)_4(dppm)]$ (3b). This compound was prepared and purified in a fashion similar to **3a** in a yield of 56%. Data for **3b**: R_f = 0.40 (THF/hexanes/Et_3N = 1/2/0.1, v/v/v). Anal. for $C_{139}H_{126}N_{16}O_{20}P_2Ru_4Co_2 \cdot H_2O$, found (calcd): C, 56.45 (56.68); H, 4.37 (4.35); N, 7.58 (7.61). Vis-NIR, λ_{max} (nm, ε(M^{-1} cm^{-1})): 950(sh), 770(13 900), 561(18 000). IR, υ/cm^{-1}: 2016 (w), 1992 (w), 1967 (w); Electrochemical, $E_{1/2}$/V, E_p/V, $i_{backward}$/$i_{forward}$: A, 0.49 (E_{pa}); B, 0.31 (E_{pc}); C, −0.87, 0.069, 0.92; D, −1.07, 0.070, 1.09.

Synthesis of $[Ru_2(^iBuOap)_4]_2(\mu$-$C_6)[Co_2(CO)_4(dppm)]$ (3c). Compound **3c** was prepared using the same procedure as that of **3a** with $[Ru_2(ap)_4]_2(\mu$-$C_6)$ being replaced by $[Ru_2(^iBuOap)_4]_2(\mu$-$C_6)$ in 65% yield. Data for **3c**: R_f = 0.31 (THF/hexanes/Et_3N = 1/3/0.1, v/v/v). Anal. for $C_{160}H_{178}N_{16}O_{17}Cl_5P_2Ru_4Co_2$, found (calcd): C, 53.97(54.35); H, 5.12 (5.07); N, 6.16(6.34). Vis-NIR, λ_{max} (nm, ε(M^{-1} cm^{-1})): 950(sh), 759(19 800), 564(25 200); IR, υ/cm^{-1}: 2016 (m), 1994 (s), 1967 (s); Electrochemical, $E_{1/2}$/V, E_p/V, $i_{backward}$/$i_{forward}$: A, 0.49 (E_{pa}); B, 0.31 (E_{pc}); C, −0.90, 0.068, 0.81; D, −1.09, 0.068, 1.27.

X-ray Data Collection, Processing, and Structure Analysis and Refinement. Crystals of **1b**, **2a**, and **3b** were grown via slow diffusion of a toluene solution with hexanes, slow evaporation of a THF solution with hexanes, and slow diffusion of a THF solution with hexanes, respectively. The X-ray intensity data for **1b** and **2a** were measured on a Bruker SMART1000 CCD-based diffractometer at room temperature and those of **3b** on a Nonius KappaCCD diffractometer at 150 K, and all using MoKα (λ = 0.71073 Å). The structures of **1b** and **2a** were solved and refined using the Bruker SHELXTL (version 5.1) software package and that of **3b** was solved by direct methods using SIR2004 and refined using the SHELX-97.[40] The asymmetric unit of **1b** contains one-half of the molecule that is related to the other half by a crystallographic inversion center and two toluene solvent molecules. The asymmetric unit of **2a** also consists of one-half of the molecule and one H_2O and two THF molecules. The asymmetric unit of **3b** contains one of the molecule and three THF solvent molecules. Relevant information on the data collection and the figures of merit of final refinement are listed in Table 3.

Computational Details. Single-point calculations (S = 3 state) on these compounds have been carried out using the DFT formalism with the spin unrestricted option as implemented in the Gaussian 03 program,[41] with the B3LYP functional. The choices of basis sets are: 3-21G for H atoms, 6-31G* basis sets for C, N, O, P, and Co atoms, and LANL2DZ basis set for Ru atoms. In all calculations, convergence was achieved when the relative change in the density matrix between successive iterations was less than 1×10^{-8}.

Spectroelectrochemistry. An OTTLE cell was used to perform the spectroelectrochemistry.[42] The cell had interior dimensions of roughly 1×2 cm with a path length of 0.2 mm and was fitted with a Ag/AgCl

reference electrode and indium−tin oxide (ITO) coated glass for the working and counter electrodes. All of the spectroelectrochemical transformations showed good reversibility (greater than 95% recovery of original complex spectrum).

■ ASSOCIATED CONTENT

Ⓢ Supporting Information. CVs of all compounds except **1a**; DPVs of compounds **1c**, **2a**, **2c**, **3a**, and **3c**; Vis-NIR spectra of **1b**, **2b**, **2c**, **3a**, and **3b** in THF; oxidation spectroelectrochemistry of **1c**, **2a** and **3c**; calculated LUMOs for compounds **1b**, **2a**, and **3b**; X-ray crystallographic files in CIF format for **1b**, **2a**, and **3b**; and the complete author list of ref 41. This material is available free of charge via the Internet at http://pubs.acs.org.

■ AUTHOR INFORMATION

Corresponding Author
tren@purdue.edu

■ ACKNOWLEDGMENT

This work was supported in part by the National Science Foundation (grants no. CHE 0715404 and CHE 1057621 to TR), Purdue University and the Natural Sciences Engineering Research Council of Canada (NSERC to R.J.C.).

■ REFERENCES

(1) (a) Barbara, P. F.; Meyer, T. J.; Ratner, M. A. *J. Phys. Chem.* **1996**, *100*, 13148. (b) Creutz, C.; Brunschwig, B. S.; Sutin, N. In *Comprehensive Coordination Chemistry II: From Biology to Nanotechnology*; McCleverty, J. A., Meyer, T. J., Ed. Elsevier/Pergamon: Oxford ; New York, 2004; (c) *Electron Transfer in Chemistry*; Balzani, V., Ed.; Wiley-VCH: Weinheim, Germany, 2001.

(2) (a) *Molecular Nanoelectronics*; Reed, M. A., Lee, T., Ed.; American Scientific Publishers: Stevenson Ranch, CA, 2003; (b) Joachim, C.; Ratner, M. A. *Proc. Natl. Acad. Sci. U.S.A.* **2005**, *102*, 8801. (c) Ulgut, B.; Abruna, H. D. *Chem. Rev.* **2008**, *108*, 2721.

(3) (a) Albinsson, B.; Martensson, J. *J. Photochem. Photobiol., C* **2008**, *9*, 138. (b) Thompson, B. C.; Frechet, J. M. J. *Angew. Chem., Int. Ed.* **2008**, *47*, 58.

(4) (a) Geiger, W. E. *Organometallics* **2007**, *26*, 5738. (b) Gray, H. B.; Winkler, J. R. *Proc. Natl. Acad. Sci. U.S.A.* **2005**, *102*, 3534. (c) Geiger, W. E. *Organometallics* **2011**, *30*, 28.

(5) (a) Paul, F.; Lapinte, C. *Coord. Chem. Rev.* **1998**, *178−180*, 431. (b) Yam, V. W.-W. *Acc. Chem. Res.* **2002**, *35*, 555. (c) Paul, F.; Lapinte, C. In *Unusual structures and physical properties in organometallic chemistry*; Gielen, M., Willem, R., Wrackmeyer, B., Ed. Wiley: West Sussex, England, 2002; (d) Szafert, S.; Gladysz, J. A. *Chem. Rev.* **2006**, *106*, 1. (e) Akita, M.; Koike, T. *Dalton Trans.* **2008**, 3523. (f) Wong, W.-Y.; Ho, C.-L. *Acc. Chem. Res.* **2010**, *43*, 1246. (g) Higgins, S. J.; Nichols, R. J.; Martin, S.; Cea, P.; van der Zant, H. S. J.; Richter, M. M.; Low, P. J. *Organometallics* **2011**, *30*, 7. (h) Zhou, G.-J.; Wong, W.-Y. *Chem. Soc. Rev.* **2011**, *40*, 2541. (i) Costuas, K.; Rigaut, S. *Dalton Trans.* **2011**, *40*, 5643.

(6) Ren, T. *Organometallics* **2005**, *24*, 4854.

(7) (a) Schull, T. L.; Kushmerick, J. G.; Patterson, C. H.; George, C.; Moore, M. H.; Pollack, S. K.; Shashidhar, R. *J. Am. Chem. Soc.* **2003**, *125*, 3202. (b) Blum, A. S.; Ren, T.; Parish, D. A.; Trammell, S. A.; Moore, M. H.; Kushmerick, J. G.; Xu, G.-L.; Deschamps, J. R.; Pollack, S. K.; Shashidhar, R. *J. Am. Chem. Soc.* **2005**, *127*, 10010. (c) Kim, B.; Beebe, J. M.; Olivier, C.; Rigaut, S.; Touchard, D.; Kushmerick, J. G.; Zhu, X.-Y.; Frisbie, C. D. *J. Phys. Chem. C* **2007**, *111*, 7521. (d) Mahapatro, A. K.; Ying, J.; Ren, T.; Janes, D. B. *Nano Lett* **2008**, *8*, 2131. (e) Lu, Y.; Quardokus, R.; Lent, C. S.; Justaud, F.; Lapinte, C.; Kandel, S. A. *J. Am. Chem. Soc.* **2010**, *132*, 13519.

(8) (a) Le Narvor, N.; Toupet, L.; Lapinte, C. *J. Am. Chem. Soc.* **1995**, *117*, 7129. (b) Hamon, P.; Justaud, F.; Cador, O.; Hapiot, P.; Rigaut, S.; Toupet, L.; Ouahab, L.; Stueger, H.; Hamon, J.-R.; Lapinte, C. *J. Am. Chem. Soc.* **2008**, *130*, 17372.

(9) Kheradmandan, S.; Heinze, K.; Schmalle, H. W.; Berke, H. *Angew. Chem., Int. Ed.* **1999**, *38*, 2270.

(10) (a) Sun, J.; Shaner, S. E.; Jones, M. K.; O'Hanlon, D. C.; Mugridge, J. S.; Hopkins, M. D. *Inorg. Chem.* **2010**, *49*, 1687. (b) Semenov, S. N.; Blacque, O.; Fox, T.; Venkatesan, K.; Berke, H. *J. Am. Chem. Soc.* **2010**, *132*, 3115.

(11) (a) Dembinski, R.; Bartik, T.; Bartik, B.; Jaeger, M.; Gladysz, J. A. *J. Am. Chem. Soc.* **2000**, *122*, 810. (b) Yam, V. W. W.; Lau, V. C. Y.; Cheung, K. K. *Organometallics* **1996**, *15*, 1740.

(12) (a) Bruce, M. I.; Low, P. J.; Costuas, K.; Halet, J.-F.; Best, S. P.; Heath, G. A. *J. Am. Chem. Soc.* **2000**, *122*, 1949. (b) Olivier, C.; Costuas, K.; Choua, S.; Maurel, V.; Turek, P.; Saillard, J.-Y.; Touchard, D.; Rigaut, S. *J. Am. Chem. Soc.* **2010**, *132*, 5638.

(13) (a) Farley, R. T.; Zheng, Q.; Gladysz, J. A.; Schanze, K. S. *Inorg. Chem.* **2008**, *47*, 2955. (b) Zheng, Q.; Bohling, J. C.; Peters, T. B.; Frisch, A. C.; Hampel, F.; Gladysz, J. A. *Chem.—Eur. J.* **2006**, *12*, 6486. (c) Zheng, Q.; Gladysz, J. A. *J. Am. Chem. Soc.* **2005**, *127*, 10508.

(14) (a) Ren, T.; Zou, G.; Alvarez, J. C. *Chem. Commun.* **2000**, 1197. (b) Ying, J.-W.; Liu, I. P.-C.; Xi, B.; Song, Y.; Campana, C.; Zuo, J.-L.; Ren, T. *Angew. Chem., Int. Ed.* **2010**, *49*, 954.

(15) Xu, G.-L.; Zou, G.; Ni, Y.-H.; DeRosa, M. C.; Crutchley, R. J.; Ren, T. *J. Am. Chem. Soc.* **2003**, *125*, 10057.

(16) (a) Fraysse, S.; Coudret, C.; Launay, J. P. *Eur. J. Inorg. Chem.* **2000**, 1581. (b) Motoyama, K.; Koike, T.; Akita, M. *Chem. Commun.* **2008**, 5812.

(17) Rocha, R. C.; Toma, H. E. *Inorg. Chem. Commun.* **2001**, *4*, 230.

(18) Gao, L.-B.; Zhang, L.-Y.; Shi, L.-X.; Chen, Z.-N. *Organometallics* **2006**, *24*, 1678.

(19) Xi, B.; Xu, G.-L.; Ying, J.-W.; Han, H.-L.; Cordova, A.; Ren, T. *J. Organomet. Chem.* **2008**, *693*, 1656.

(20) Zhang, L.; Xi, B.; Liu, I. P. C.; Choudhuri, M. M. R.; Crutchley, R. J.; Updegraff, J. B.; Protasiewicz, J. D.; Ren, T. *Inorg. Chem.* **2009**, *48*, 5187.

(21) Xi, B.; Zhang, L.; Liu, I. P. C.; Choudhuri, M. M. R.; Crutchley, R. J.; Ren, T., manuscript in preparation.

(22) Bruce, M. I. *Aust. J. Chem.* **2011**, *64*, 77.

(23) (a) Masai, H.; Sonogash., K; Hagihara, N. *J. Organomet. Chem.* **1972**, *34*, 397. (b) Onuma, K.; Kai, Y.; Yasuoka, N.; Kasai, N. *Bull. Chem. Soc. Jpn.* **1975**, *48*, 1696. (c) Bruce, M. I.; Hambley, T. W.; Snow, M. R.; Swincer, A. G. *Organometallics* **1985**, *4*, 494. (d) Bruce, M. I.; Cole, M. L.; Parker, C. R.; Skelton, B. W.; White, A. H. *Organometallics* **2008**, *27*, 3352. (e) Onitsuka, K.; Ose, N.; Ozawa, F.; Takahashi, S. *J. Organomet. Chem.* **1999**, *578*, 169.

(24) (a) Bruce, M. I.; Low, P. J.; Skelton, B. W.; White, A. H. *New J. Chem.* **1998**, *22*, 419. (b) Bruce, M. I.; Low, P. J.; Hartl, F.; Humphrey, P. A.; de Montigny, F.; Jevric, M.; Lapinte, C.; Perkins, G. J.; Roberts, R. L.; Skelton, B. W.; White, A. H. *Organometallics* **2005**, *24*, 5241.

(25) Bruce, M. I.; Humphrey, P. A.; Jevric, M.; Skelton, B. W.; White, A. H. *J. Organomet. Chem.* **2007**, *692*, 2564.

(26) (a) Rubin, Y.; Knobler, C. B.; Diederich, F. *J. Am. Chem. Soc.* **1990**, *112*, 4966. (b) Low, P. J.; Rousseau, R.; Lam, P.; Udachin, K. A.; Enright, G. D.; Tse, J. S.; Wayner, D. D. M.; Carty, A. J. *Organometallics* **1999**, *18*, 3885. (c) Tanaka, Y.; Koike, T.; Akita, M. *Eur. J. Inorg. Chem.* **2010**, 3571.

(27) Mochida, T.; Yamazaki, S. *J. Chem. Soc., Dalton Trans.* **2002**, 3559.

(28) Crutchley, R. J. *Adv. Inorg. Chem.* **1994**, *41*, 273.

(29) (a) Geiger, W. E.; Barriere, F. *Acc. Chem. Res.* **2010**, *43*, 1030. (b) Barrière, F.; Camire, N.; Geiger, W. E.; Mueller-Westerhoff, U. T.; Sanders, R. *J. Am. Chem. Soc.* **2002**, *124*, 7262. (c) Noviandri, I.; Brown, K. N.; Fleming, D. S.; Gulyas, P. T.; Lay, P. A.; Masters, A. F.; Phillips, L. *J. Phys. Chem. B* **1999**, *103*, 6713.

(30) Xu, G.-L.; Cordova, A.; Ren, T. *J. Cluster Sci.* **2004**, *15*, 413.

(31) (a) Miskowski, V. M.; Loehr, T. M.; Gray, H. B. *Inorg. Chem.* **1987**, *26*, 1098. (b) Miskowski, V. M.; Gray, H. B. *Inorg. Chem.* **1988**, *27*, 2501.
(32) Hush, N. S. *Prog. Inorg. Chem.* **1967**, *8*, 391.
(33) Brunschwig, B. S.; Creutz, C.; Sutin, N. *Chem. Soc. Rev.* **2002**, *31*, 168.
(34) Ren, T.; Xu, G.-L. *Comm. Inorg. Chem.* **2002**, *23*, 355.
(35) (a) Ward, M. D. *Chem. Soc. Rev.* **1995**, *24*, 121. (b) Aquino, M. A. S.; Lee, F. L.; Gabe, E. J.; Bensimon, C.; Greedan, J. E.; Crutchley, R. J. *J. Am. Chem. Soc.* **1992**, *114*, 5130.
(36) (a) Lichtenberger, D. L.; Renshaw, S. K.; Wong, A.; Tagge, C. D. *Organometallics* **1993**, *12*, 3522. (b) Lichtenberger, D. L.; Renshaw, S. K.; Bullock, R. M. *J. Am. Chem. Soc.* **1993**, *115*, 3276.
(37) (a) Solomon, G. C.; Andrews, D. Q.; Van Duyne, R. P.; Ratner, M. A. *J. Am. Chem. Soc.* **2008**, *130*, 7788. (b) Solomon, G. C.; Andrews, D. Q.; Goldsmith, R. H.; Hansen, T.; Wasielewski, M. R.; Van Duyne, R. P.; Ratner, M. A. *J. Am. Chem. Soc.* **2008**, *130*, 17301.
(38) Chia, L. S.; Cullen, W. R. *Inorg. Chem.* **1975**, *14*, 482.
(39) Rubin, Y.; Lin, S. S.; Knobler, C. B.; Anthony, J.; Boldi, A. M.; Diederich, F. *J. Am. Chem. Soc.* **1991**, *113*, 6943.
(40) Sheldrick, G. M. *Acta Cryst. A* **2008**, *64*, 112.
(41) Frisch, M. J. et al. *Gaussian 03*, revision D.02, Gaussian, Inc.: Wallingford, CT, 2003.
(42) Krejcik, M.; Danek, M.; Hartl, F. *J. Electroanal. Chem.* **1991**, *317*, 179.